APPLICATION OF EARTHQUAKE MECHANISM STUDIES

Hiroo Kanamori

Seismological Laboratory, 252-21
California Institute of Technology
Pasadena, California 91125

USGS CONTRACT NO. 14-08-0001-18321
Supported by the EARTHQUAKE HAZARDS REDUCTION PROGRAM

OPEN-FILE NO.81-281

Introduction

In this final technical report, we summarize the results of our investigations on "Application of Earthquake Mechanism Studies to Prediction of Long-Period Ground Motion and Related Problems". As we stated in our proposal, the primary purpose of this project is to conduct reconaissance studies on the local magnitude, M_L, of very large earthquakes, and complexity of large multiple shocks. Since the results obtained for the period from 1 October 1979 to 31 March 1980 have been reported in the Semi-Annual Technical Report of this contract, this report contains mainly the results obtained during the period from 1 April, 1980 to September 30, 1980.

Investigations

1. Study of Body Waves of Great Earthquakes.

The complexity of the faulting process of an earthquake has dominating effects on the nature of strong ground motions resulting from it. Unfortunately, very little is known about the nature of complexity, particularly of very large earthquakes. We investigated the body waves from very large earthquakes in an attempt to understand the nature of complexity.

2. Development of an Analysis Method of Complex Events.

There is no standard method with which we can interpret complex events in terms of the seismic moment and the stress drop of the constituent events of a multiple shock. We developed a method which deconvolves observed seismograms into a series of discrete events.

Results

1. Study of Body Waves of Great Earthquakes.

There is considerable variation in the size of the largest earthquakes amongst the subduction zones (see Figure 1). With the asperity model, the seismic coupling between the downgoing and overlying plates occurs where the asperities of either side are in contact. A larger asperity contact area results in a stronger coupling, and this could cause larger earthquakes. Thus, the regional variation in the seismic coupling of subduction zones can be interpreted as differences in the distribution of asperities on the fault plane.

If we consider asperities as strong regions on the fault plane which break in sequence during an earthquake, we might expect to observe a series of energetic arrivals instead of one large smooth arrival. As the total time of the earthquake rupture process is less than 20 sec (for up to magnitude 8 events), it is necessary to use body waves to distinguish the irregular character of the source process. The concept of multiple shocks has been used to explain the complicated body waves from larger events (e. g. Kanamori and Stewart, 1978), and these multiple shocks have been interpreted as the breaking of asperities. We have extended these considerations to the great earthquakes in order to examine the asperity coupling model of subduction thrust events.

Three of the largest earthquakes in this century are: Kurile Is., M_w = 8.5, Alaska, M_w = 9.2, 1964, and Rat Is., M_w = 8.7, 1965. These events were recorded by the WWSSN network with the 30-100 long period instruments. The body waves of these large events are compared to those of the Niigata earthquake, a "standard magnitude 8" event. As the body waves for these great earthquakes are off scale at nearly all of the stations in the teleseismic range (Δ= 30 to 80 deg.), seismograms recorded in the core shadow zone are used. Diffraction around the core

serves to attenuate the amplitudes such that the body waves are on scale sufficiently far into the shadow. The diffraction effect filters out the higher frequencies, however the effect on the waveforms is small compared to the differences between the earthquakes. Figures 2 through 5 show the focal mechanisms determined for those events and also plot the departure points of the P-waves. All of the subduction events are shallow thrust events, and the Niigata event has a similar mechanism although it occurred on the western side of Japan and does not represent the active subduction of oceanic lithosphere. Though some of the P-waves are nearly nodal, the maximum amplitude of the observed waveforms should still be representative of the earthquake size due to the pP and sP arrivals. This is demonstrated in Figure 6 where the peak to peak relative amplitudes of synthetic seismograms computed for a shallow thrust mechanism are plotted on the focal sphere. Notice that the total range in the peak to peak amplitudes is slightly larger than a factor of two.

Seismograms from each event are plotted in Figures 7 through 10, all normalized to a magnification of 1500. Two seismograms from each event, representative of the distance range, are plotted together in Figure 11. One striking feature of Figure 11 is that the Alaskan earthquake has a substantially larger body wave amplitude than the other earthquakes. The long period seismic moment of the Alaskan event is a factor of: 6.6 larger than the Rat Is. event, 12 larger than the Kurile Is. event, and 273 larger than the Niigata event. The total source process time for the larger events is several minutes long. The source process time of the Alaskan event was estimated to be $\sim$ 300 sec by Kanamori (1970) based

on surface wave observations. For the Niigata event, there is basically a single pulse. This pulse has been analyzed as consisting of at least two distinct events (Hirasawa, 1965), however it is a single break when considered at the time scale of interest here. An important feature that we wish to emphasize is the broad pulse width of the Alaskan earthquake. The first arrival in the Alaskan records has a pulse width of $\sim$ 30 sec. This broad pulse requires a ramp-type time function of at least 30 sec duration, and assuming a symmetric trapezoidal time function, the total time function would be greater than 60 sec in length. Thus, this pulse requires a time constant greater than 30 sec, and using a rupture velocity of 3.5 km/sec we conclude that the source length scale is greater than 100 km, and possibly 200 km. For comparison, the total time function duration of the Niigata event is less than 20 sec, and this corresponds to a source length scale of $\sim$ 30 km. Notice that the dominant periods of the Kurile Is. and Rat Is. events are intermediate to those of the Alaskan and Niigata events.

In conclusion, it seems that the source region of the initial break in the Alaskan earthquake had a length scale greater than 100 km, and that the following multiple events had a similar length scale. This length scale is substantially larger than that for Niigata earthquake, which indicates that a great earthquake is <u>not</u> just a sequence of magnitude 8 events. The dominant periods of the Kurile Is. and Rat Is. events suggest that their characteristic length scales are between the Alaskan and Niigata values. Thus, it appears that a larger asperity length scale is associated with the largest earthquakes.

2. Development of an Analysis Method of Complex Events.

We assume that all the constituent events of a multiple shock have identical geometrical parameters, the strike, dip, and rake angles. We use the parameters determined from the first-motion data. The only unknown is the source time function. Presumably the individual events of a multiple event have different time constants such as the rise time, process time and fall-off time. However, it is extremely difficult to resolve these values in complicated waveforms. For this reason, we further assume that the far-field source time function can be decomposed into unit ramp functions with an identical rise time τ.

Let $s(t)$ be the synthetic wavelet for the unit ramp function, and m_i and t_i be the magnitude and the onset time of the i-th ramp function. Then the synthetic waveform is given by:

$$S(t) = \sum_{i=1}^{N} s(t-t_i)m_i \tag{1}$$

where N is the total number of the ramp function. The values of m_i and t_i are determined by minimizing the estimation error defined by:

$$E = \int [\chi(t) - S(t)]^2 \, dt \tag{2}$$

where $\chi(t)$ is the observed wave form.

First we take a ramp function with the amplitude m_1 and the onset time t_1 for $S(t)$, and minimize E. The onset time t_1 is obtained by maximizing $|r_{s\chi}(t_1)|$, and the amplitude m_1 is determined by:

$$m_1 = r_{s\chi}(t_1)/r_s(0) \tag{3}$$

where $r_{s\chi}(t)$ is the cross-covariance of s(t) with $\chi(t)$ and $r_s(t)$ is the auto-covariance of s(t). Next, we subtract $m_1 s(t-t_1)$ from $\chi(t)$, and apply the same procedure to $\chi(t) - m_1 s(t-t_1)$ to obtain the second ramp function (m_2, t_2). The procedure is repeated until the residual or the estimation error defined by (2) does not change significantly any longer.

In this analysis, the constituent ramp functions are determined in the order of decreasing magnitude. Hence the n largest functions are in general obtained by n iterations. After n times of iteration, the estimation error is given by:

$$E_n = r_\chi(0) - r_s(0) \; [m_1^2 + \ldots + m_n^2] \qquad (4)$$

E_n is computed for various values of τ for a fixed value of n. The value of τ which minimizes E_n is used for the later analysis. Once the appropriate time constant τ is determined, the sequence of the ramp functions can be calculated by the above interation.

For the actual calculation, the effects of surface reflections near the source, attenuation, geometrical spreading, receiver function and the instrument response are included.

We applied this method to two large earthquakes: the Guatemala earthquake, February 4, 1976 (hereafter denoted by G), and the Turkey earthquake November 24, 1976 (hereafter denoted by T). Both are shallow and complex multiple events. The strike, dip and rake angles of the fault plane were taken from Kanamori and Stewart (1978) for G and Toksöz et al. (1978) for T (see Table 1).

In order to determine the rise time τ, we took stations NUR for G and AAM for T. First, a point source is located at a depth of 5 km in a semi-infinite elastic medium, and the basic wavelets were calculated with the

value of τ varied parametrically from 0.5 to 6 sec. Next, the observed seismograms were deconvolved into each wavelet and the pulse sequence. Then the estimation error was obtained after 20 iterations. In Figure 12, the values of E_{20} normalized to $r_x(0)$ are plotted against the time constant t. From the criterion that E_{20} is minimum, we obtained the optimum time constant as follows:

τ = 3 sec for G

τ = 2 sec for T

Next, fixing the time constant and the number of iterations (n = 20), we deconvolved the seismograms at other stations. The results are shown in Figure 13 for G where the time sequence of sub-events is plotted below each synthetic record.

The sequence of spikes obtained for the individual station is convolved with the unit ramp function used for the analysis to obtain the far-field wave form. Figure 14 compares the results obtained for the five stations used for the Guatemala earthquake. In this figure, long-period trends which cannot be resolved by the present analysis have been removed. Five sub-events are identified and indicated by dotted lines. The correspondence of sub-events from station to station is very good. Moremover, for some events, the onset time can be seen to change systematically with the azimuth of stations. From the area under the far-field time function for the individual event, the seismic moment of the individual event can be estimated as shown by Table 1.

TABLE 1

Seismic Moment of Individual Events

Unit: $\times 10^{26}$ dyne-cm

Station	Event: 1	2	3	4	5	Total
KEV	5.0	8.8	6.3	9.6	8.0	37.7
NUR	2.3	4.7	7.3	4.4	7.5	26.2
KTG	5.9	3.6	8.4	8.4	7.5	33.8
COP	6.3	7.2	8.8	11.5	5.9	39.7
STU	2.8	8.0	4.9	5.0	7.0	27.7
Mean	4.5	6.5	7.1	7.8	7.2	33.0
Variance	$\pm$1.3	$\pm$2.2	$\pm$1.6	$\pm$3.0	$\pm$0.3	$\pm$6.0

$$\sum M_o = (3.3 \pm .6) \times 10^{27} \text{ dyne-cm}$$

Figure Captions

Figure 1. Location of great earthquakes studied.

Figure 2. Focal mechanism of the Niigata earthquake and the locations of the stations used.

Figure 3. Focal mechanisms of the Kurile Is. earthquake and the locations of the stations used.

Figure 4. Focal mechanism of the Rat Is. earthquake and the locations of the stations used.

Figure 5. Focal mechanism of the Alaskan earthquake and the locations of the stations used.

Figure 6. Peak-to-peak amplitude of synthetic P-waves for a low-angle thrust mechanism.

Figure 7. Observed P-wave forms (Niigata earthquake).

Figure 8. Observed P-wave forms (Kurile Is. earthquake).

Figure 9. Observed P-wave forms (Rat Is. earthquake).

Figure 10. Observed P-wave forms (Alaskan earthquake).

Figure 11. Comparison of P-wave forms.

Figure 12. Estimation error as a function of τ.

Figure 13a to e. Observed seismograms of the 1976 Guatemala earthquake (top) and the deconvolved pulse sequence (the second from the bottom). The second trace is the synthetic seismograms computed by using the deconvolved pulse sequence.

Figure 14. Comparison of deconved far-field time function.

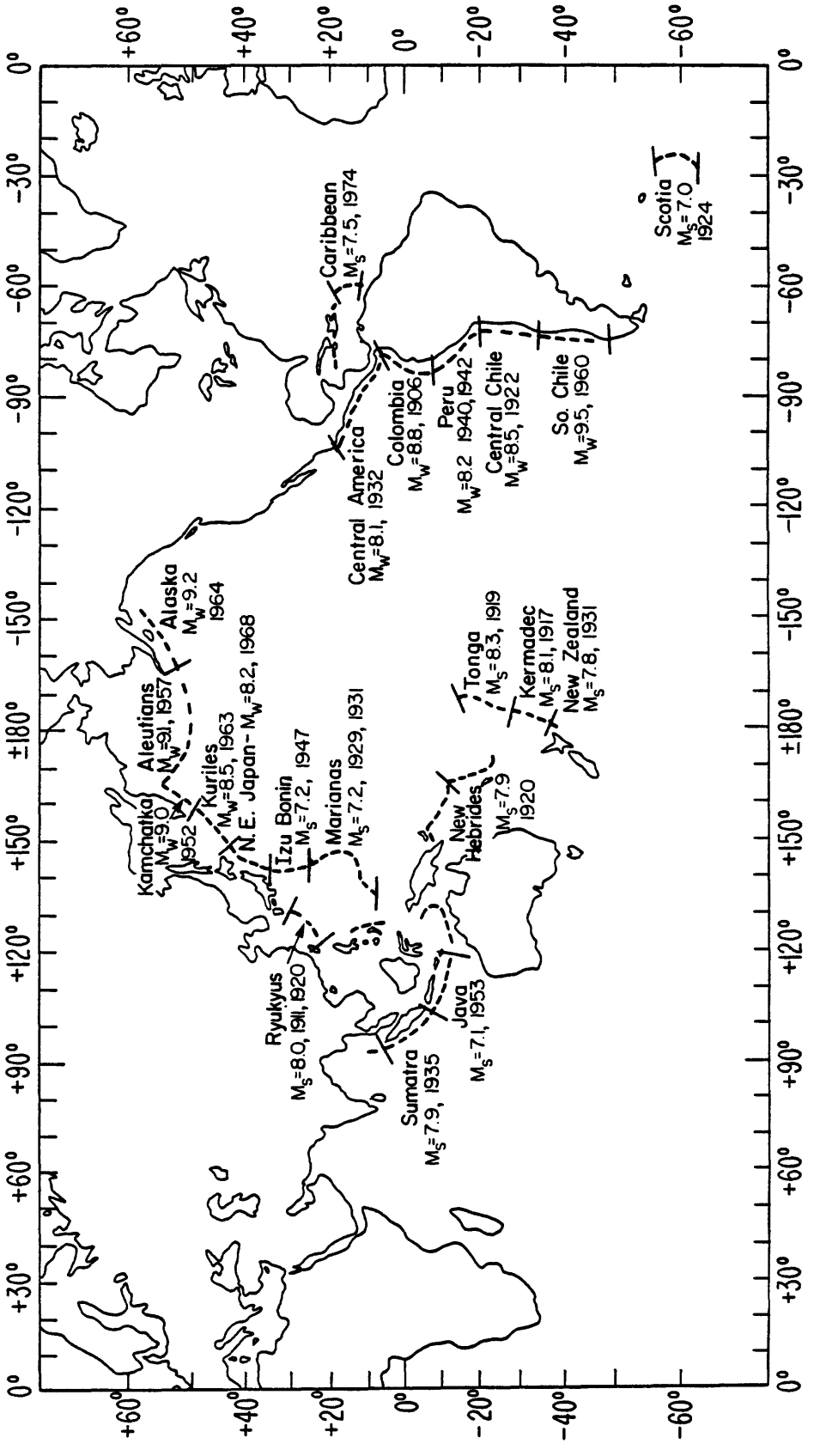
Kamchatka
M_w=9.0
1952
Aleutians
M_w=9.1, 1957
Alaska
M_w=9.2
1964
Kuriles
M_w=8.5, 1963
N.E. Japan - M_w=8.2, 1968
Izu Bonin
M_s=7.2, 1947
Marianas
M_s=7.2, 1929, 1931
Ryukyus
M_s=8.0, 1911, 1920
Sumatra
M_s=7.9, 1935
Java
M_s=7.1, 1953
New Hebrides
M_s=7.9
1920
Tonga
M_s=8.3, 1919
Kermadec
M_s=8.1, 1917
New Zealand
M_s=7.8, 1931
Central America
M_w=8.1, 1932
Caribbean
M_s=7.5, 1974
Colombia
M_w=8.8, 1906
Peru
M_w=8.2 1940, 1942
Central Chile
M_w=8.5, 1922
So. Chile
M_w=9.5, 1960
Scotia
M_s=7.0
1924

Fig. 1

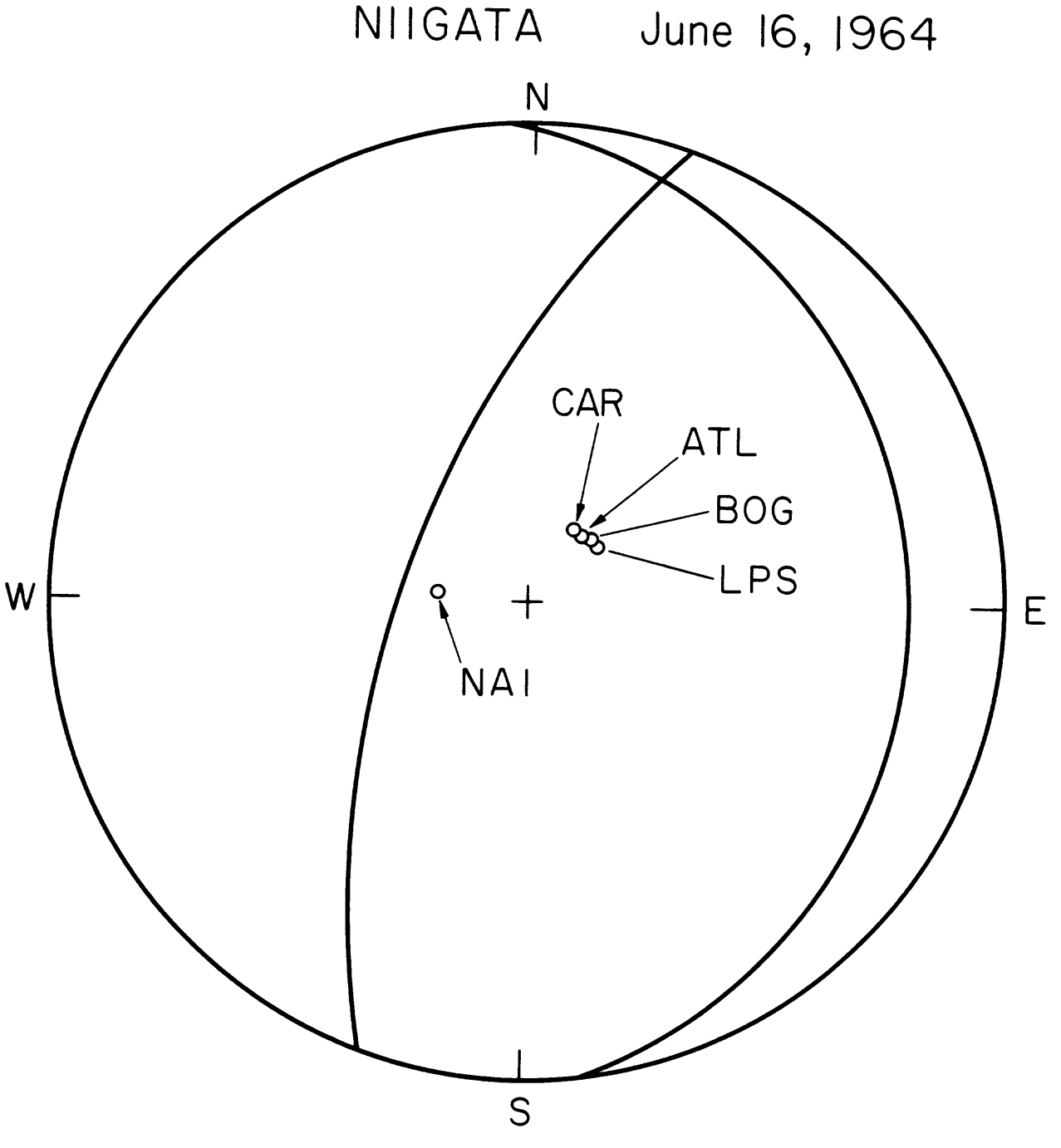

Figure 2

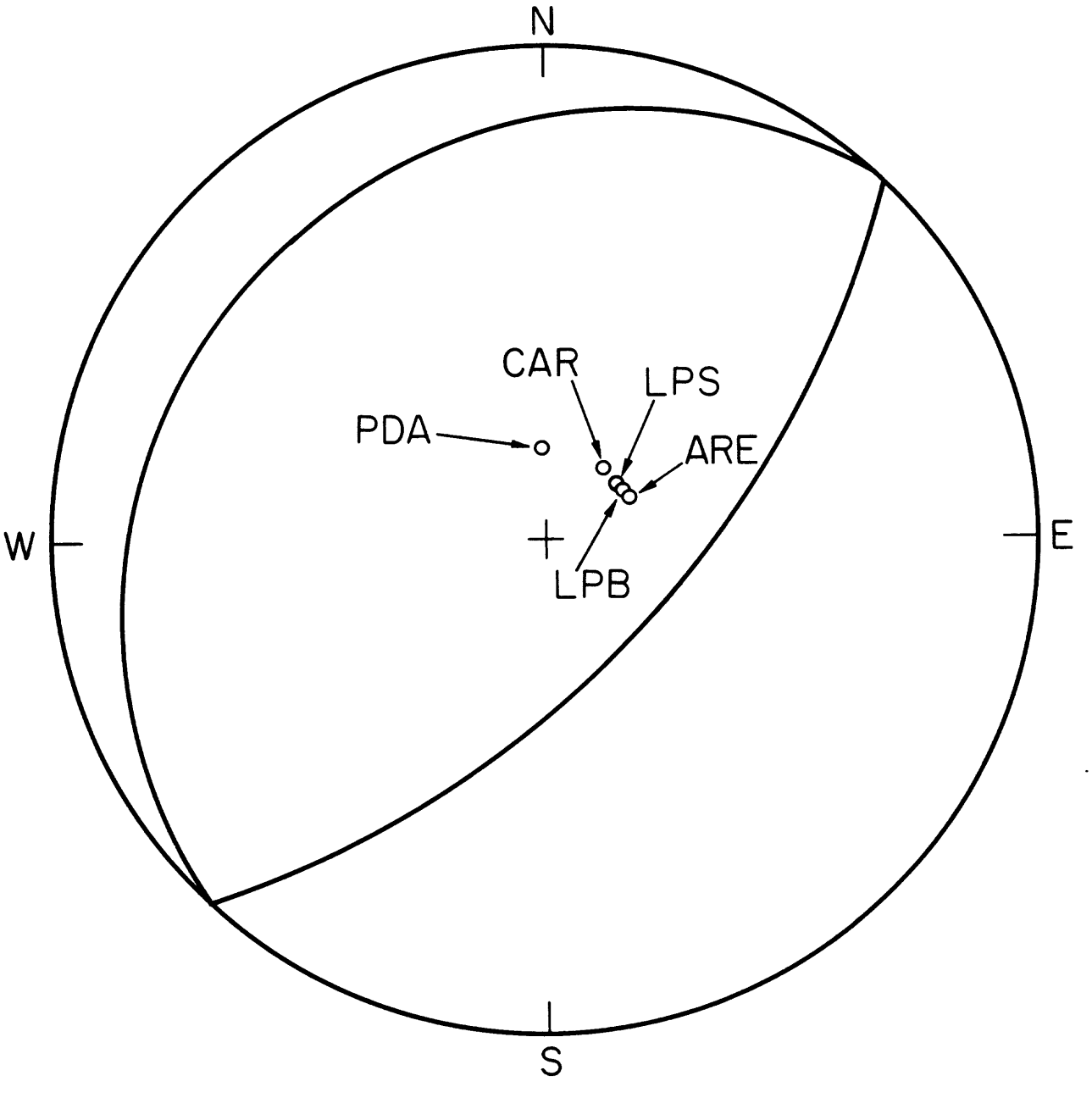

Figure 3

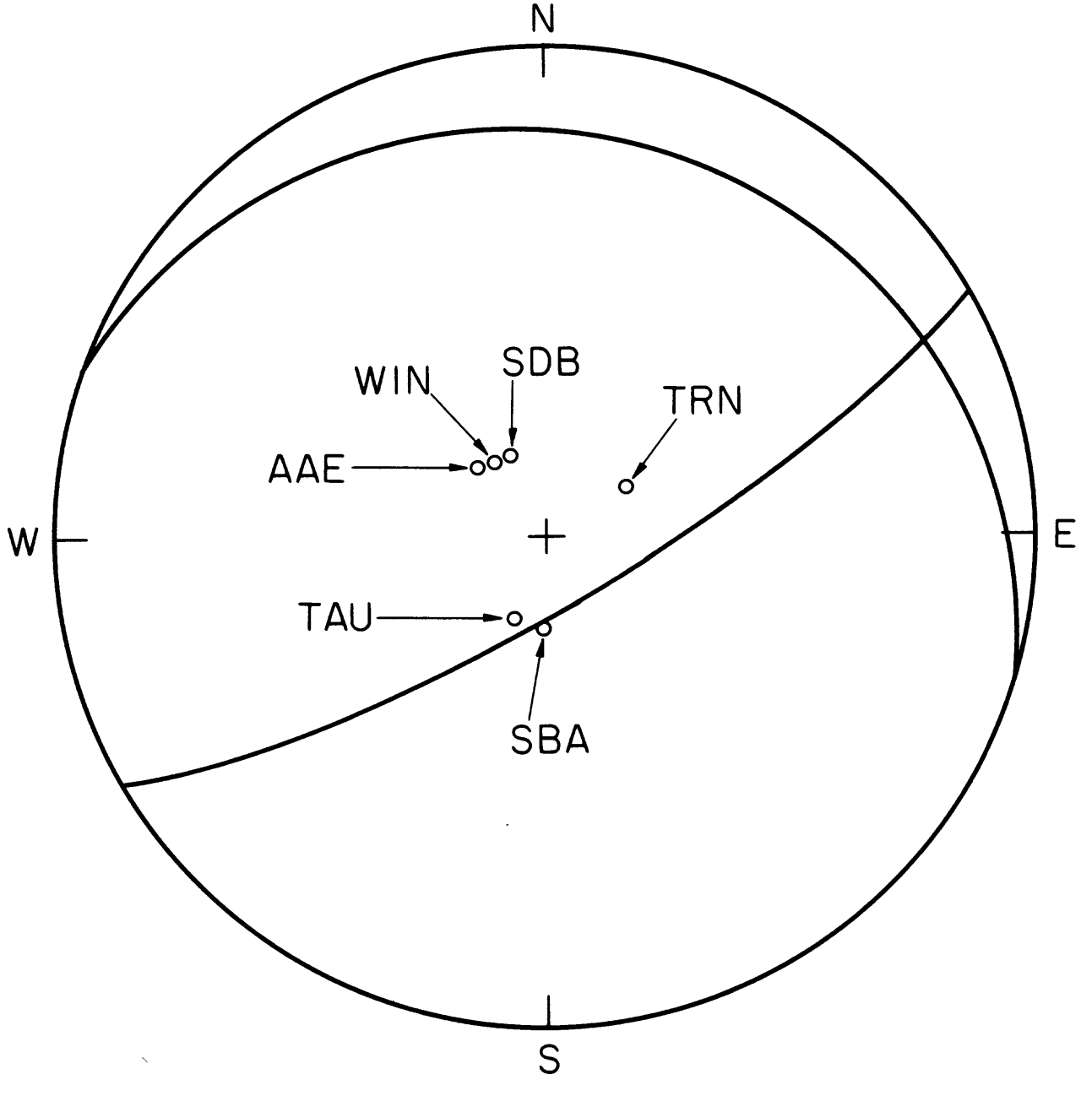

Figure 4

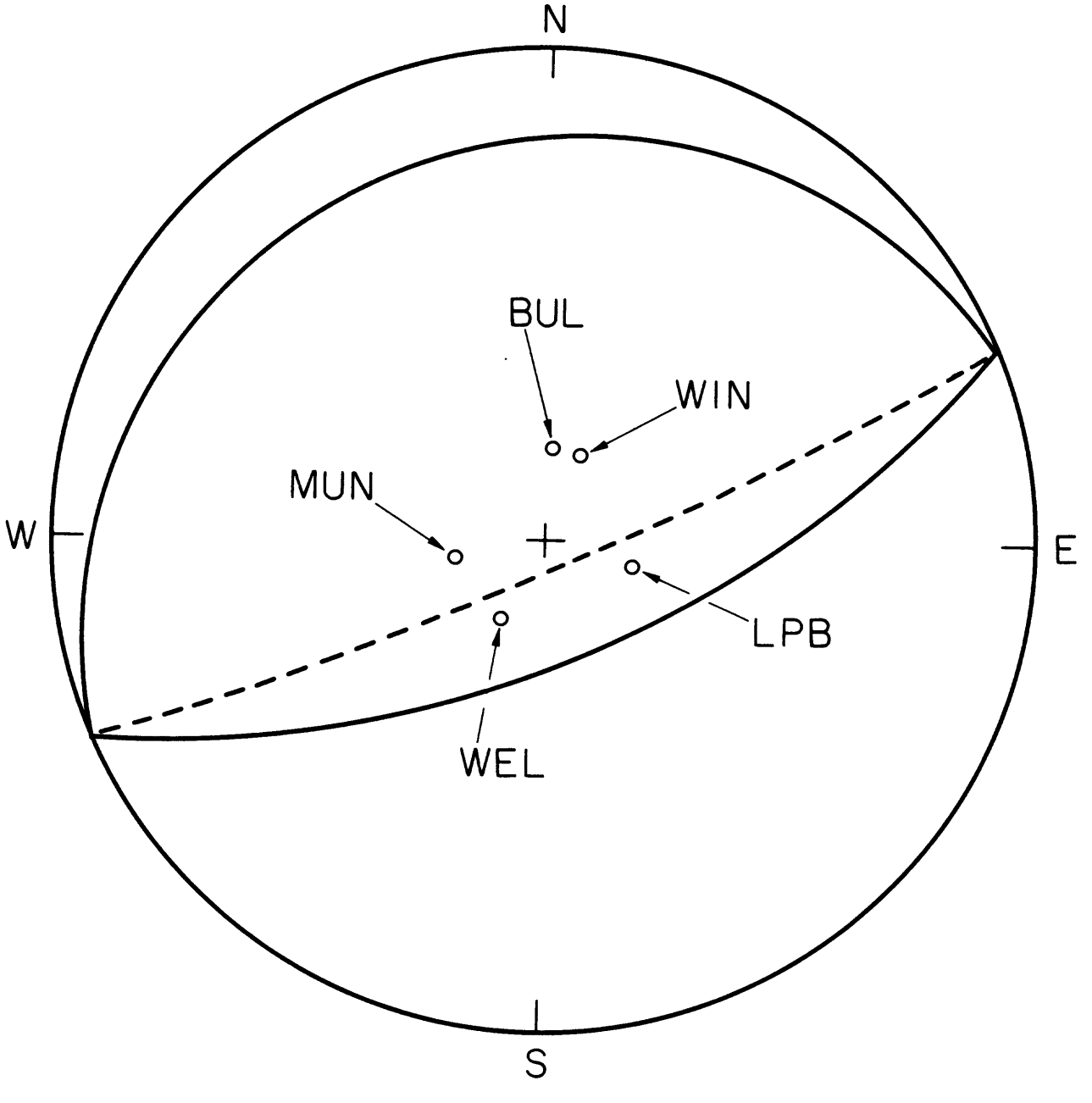

Figure 5

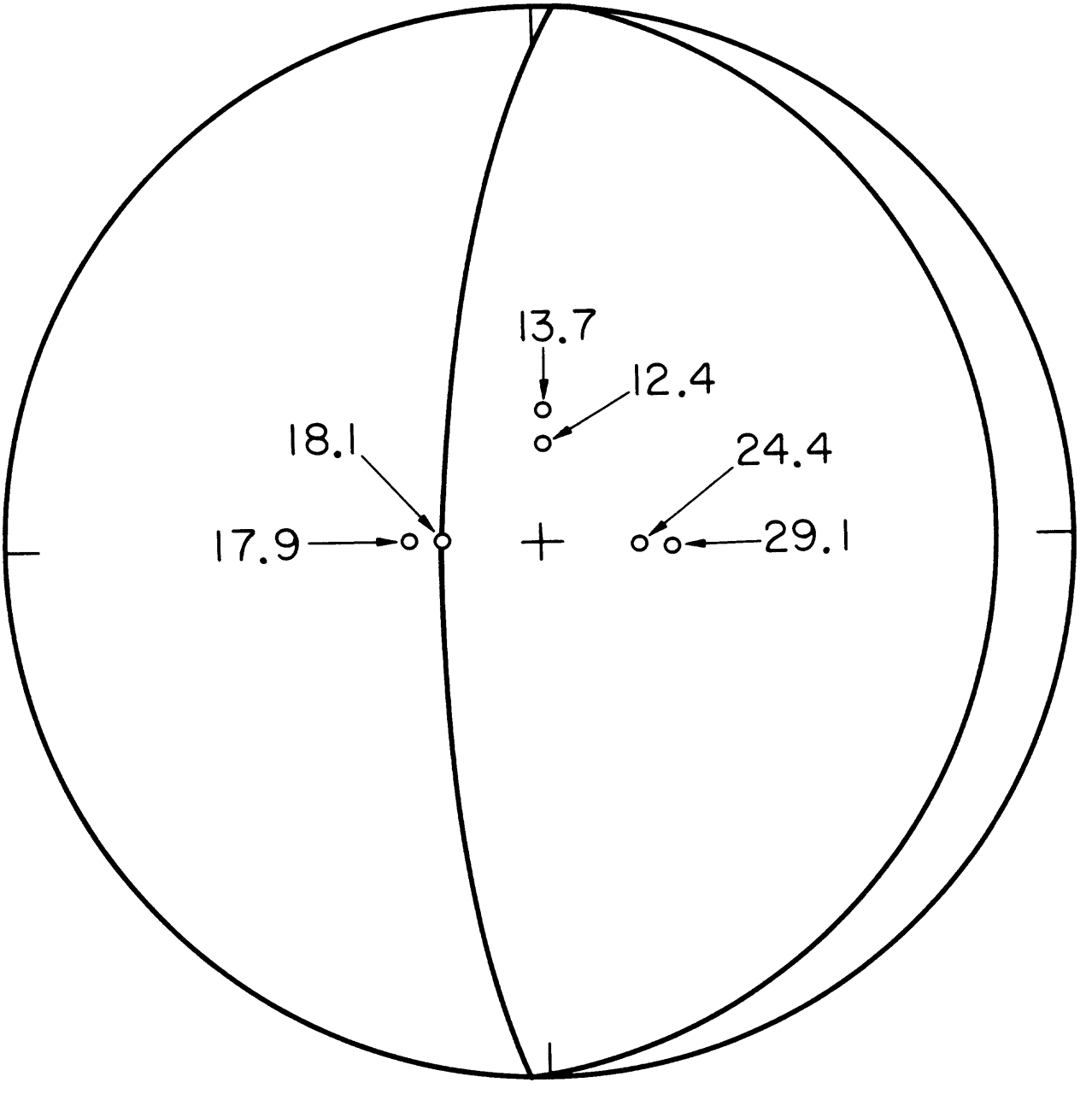

Figure 6

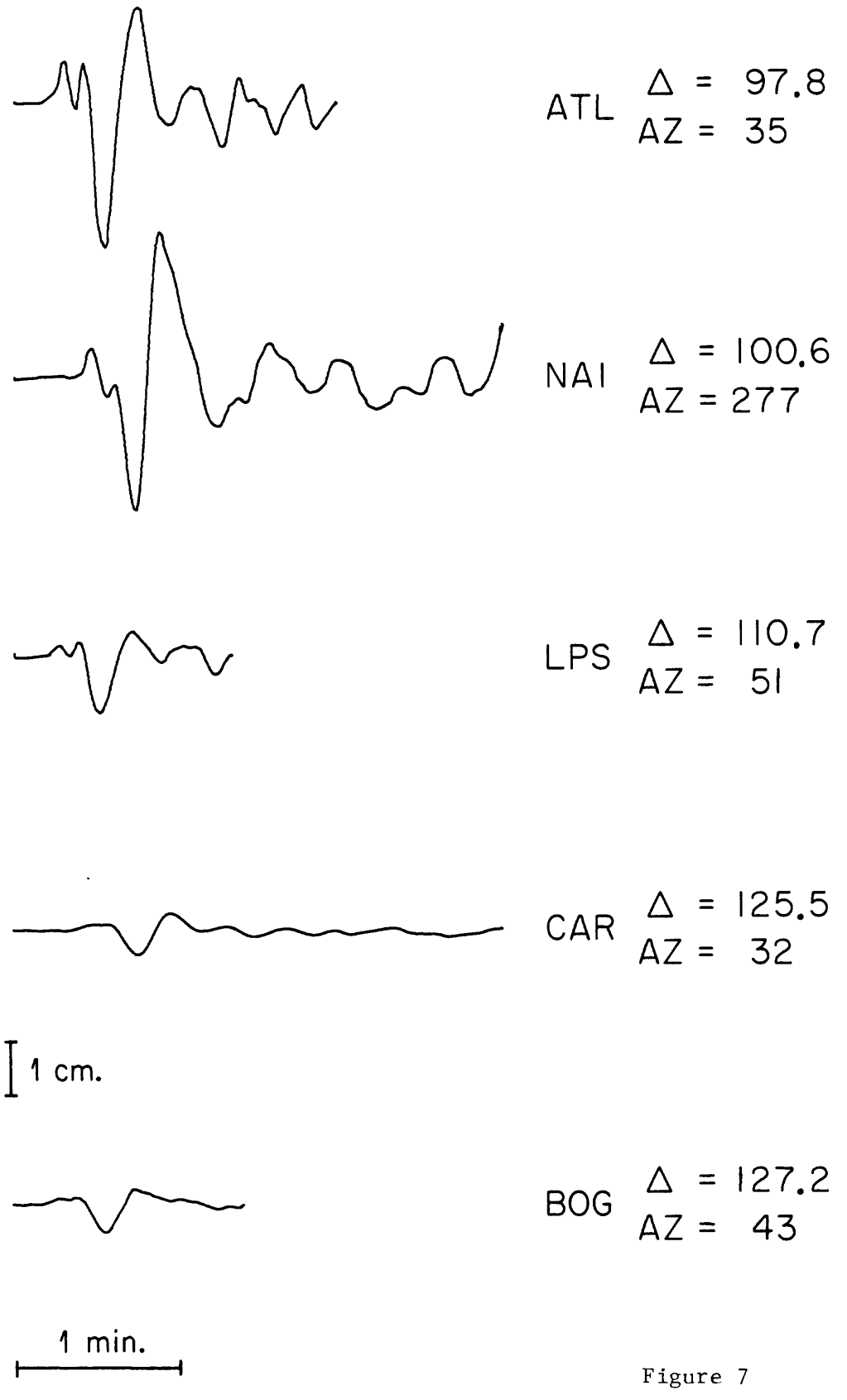
NIIGATA Jun. 16, 1964
ATL
Δ = 97.8
AZ = 35
NAI
Δ = 100.6
AZ = 277
LPS
Δ = 110.7
AZ = 51
CAR
Δ = 125.5
AZ = 32
1 cm.
BOG
Δ = 127.2
AZ = 43
1 min.

Figure 7

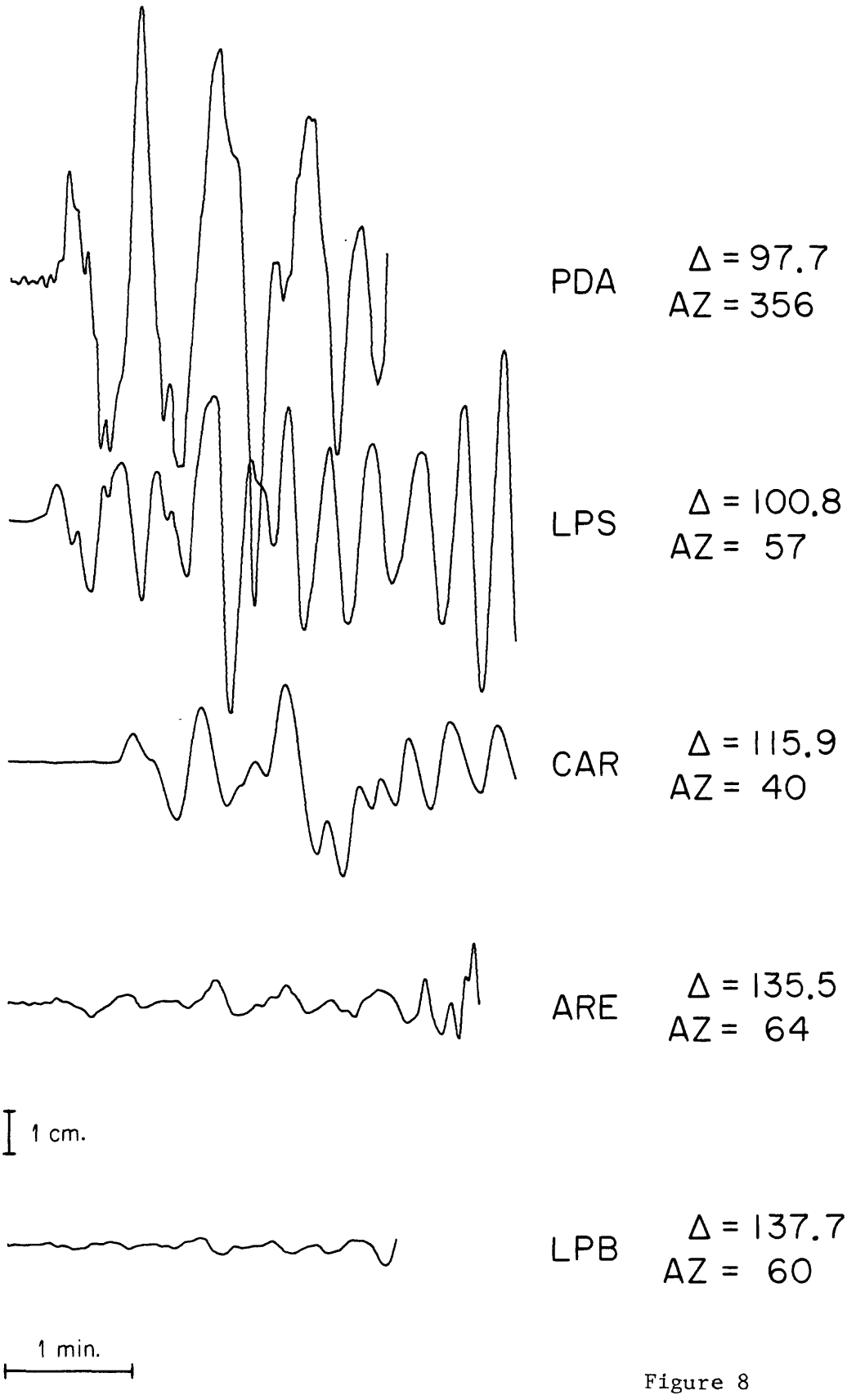
KURILE IS. Oct. 13, 1963
PDA
Δ = 97.7
AZ = 356
LPS
Δ = 100.8
AZ = 57
CAR
Δ = 115.9
AZ = 40
ARE
Δ = 135.5
AZ = 64
1 cm.
LPB
Δ = 137.7
AZ = 60
1 min.

Figure 8

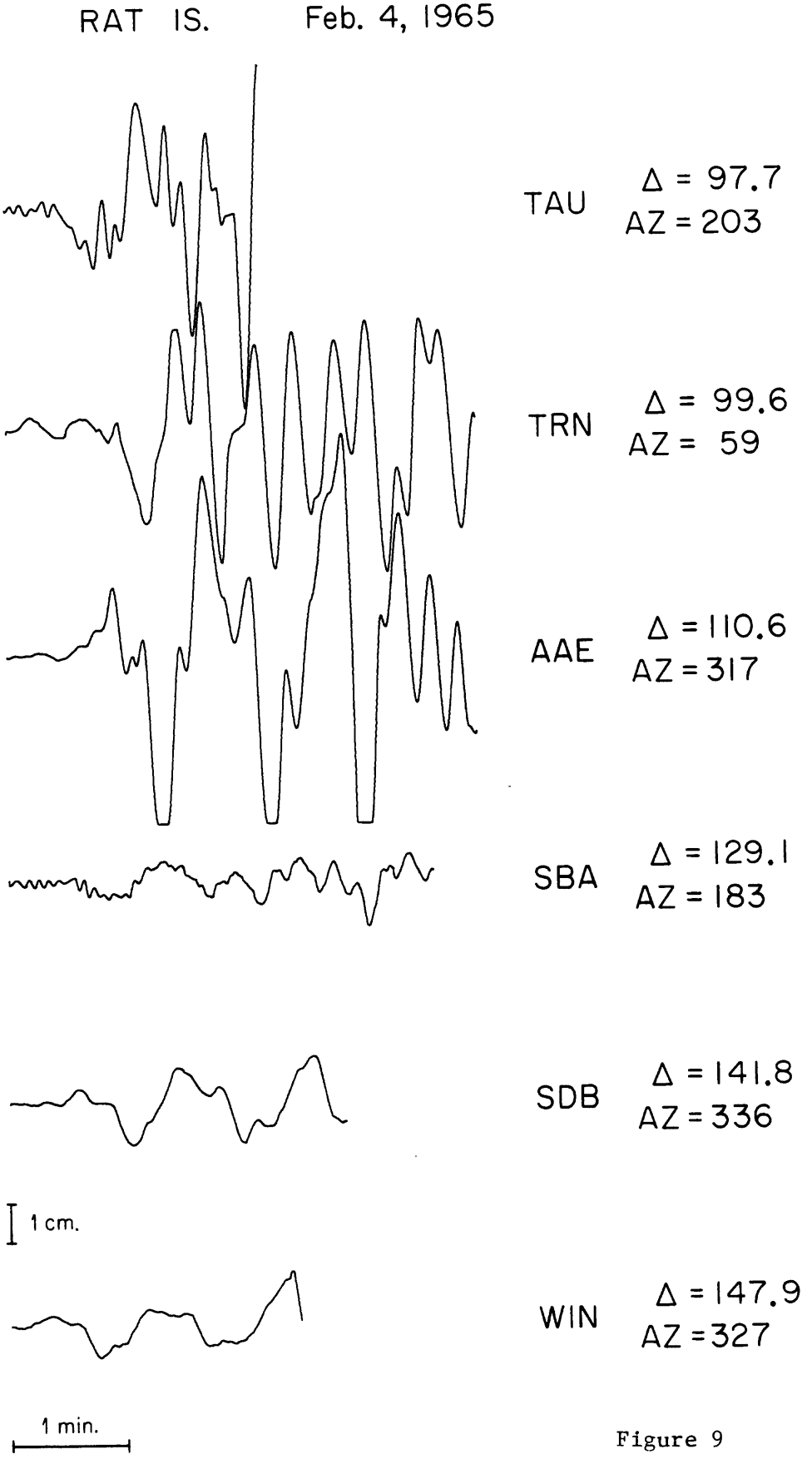
RAT IS. Feb. 4, 1965
TAU
Δ = 97.7
AZ = 203
TRN
Δ = 99.6
AZ = 59
AAE
Δ = 110.6
AZ = 317
SBA
Δ = 129.1
AZ = 183
SDB
Δ = 141.8
AZ = 336
1 cm.
WIN
Δ = 147.9
AZ = 327
1 min.

Figure 9

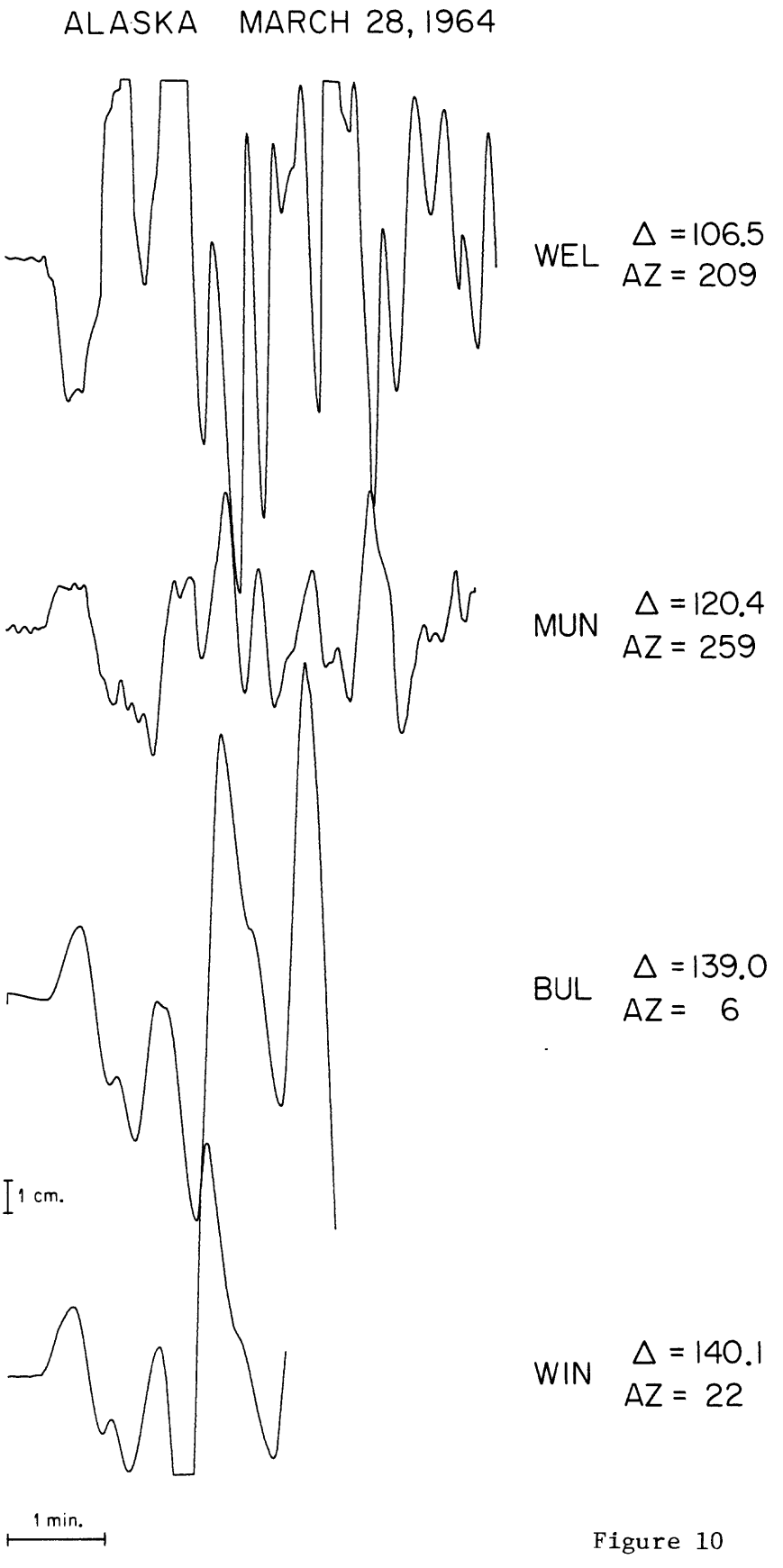
ALASKA MARCH 28, 1964
WEL
Δ = 106.5
AZ = 209
MUN
Δ = 120.4
AZ = 259
BUL
Δ = 139.0
AZ = 6
WIN
Δ = 140.1
AZ = 22
1 cm.
1 min.

Figure 10

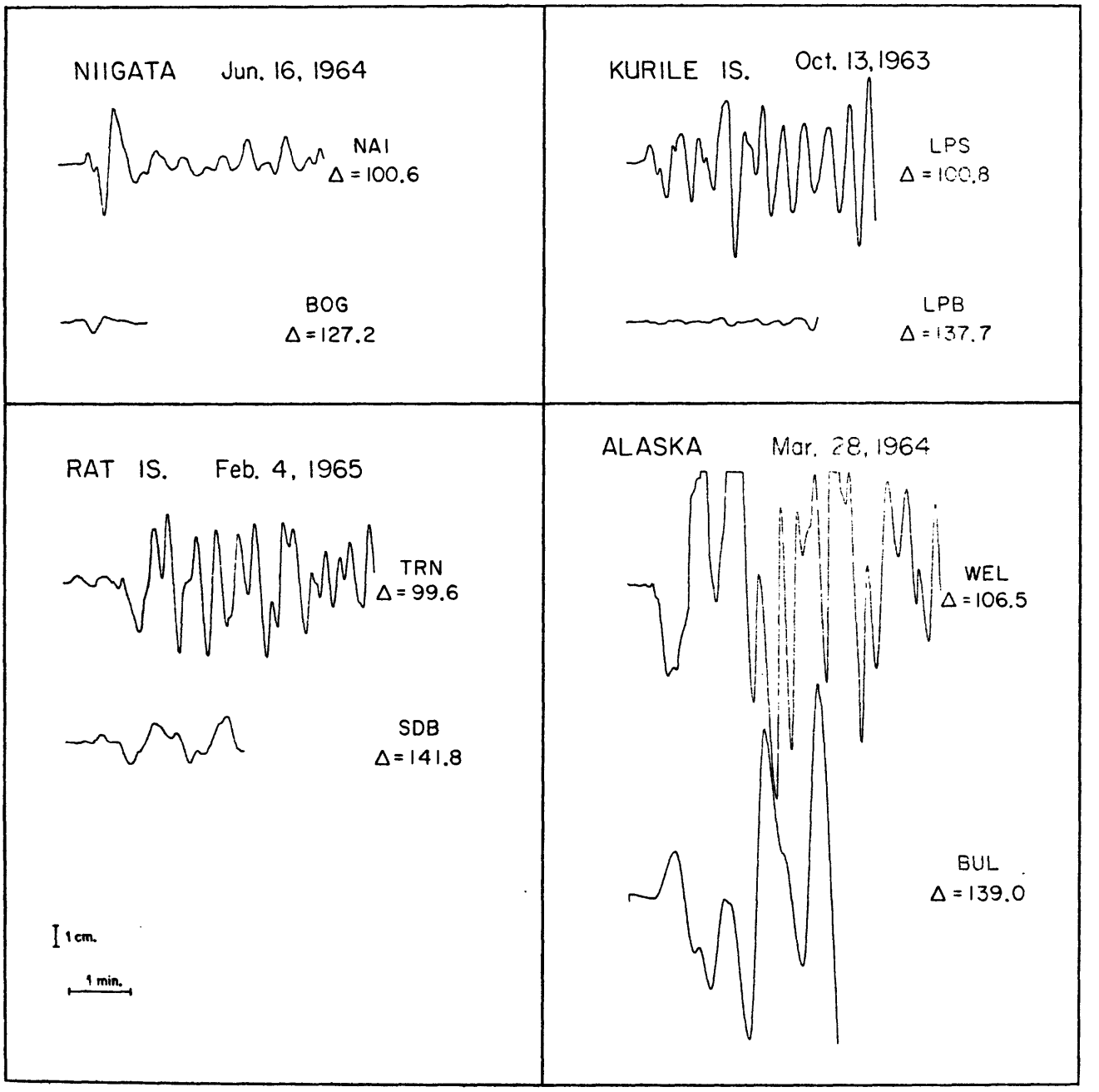
NIIGATA Jun. 16, 1964
NAI
Δ = 100.6
BOG
Δ = 127.2
KURILE IS. Oct. 13, 1963
LPS
Δ = 100.8
LPB
Δ = 137.7
RAT IS. Feb. 4, 1965
TRN
Δ = 99.6
SDB
Δ = 141.8
1 cm.
1 min.
ALASKA Mar. 28, 1964
WEL
Δ = 106.5
BUL
Δ = 139.0

Figure 11

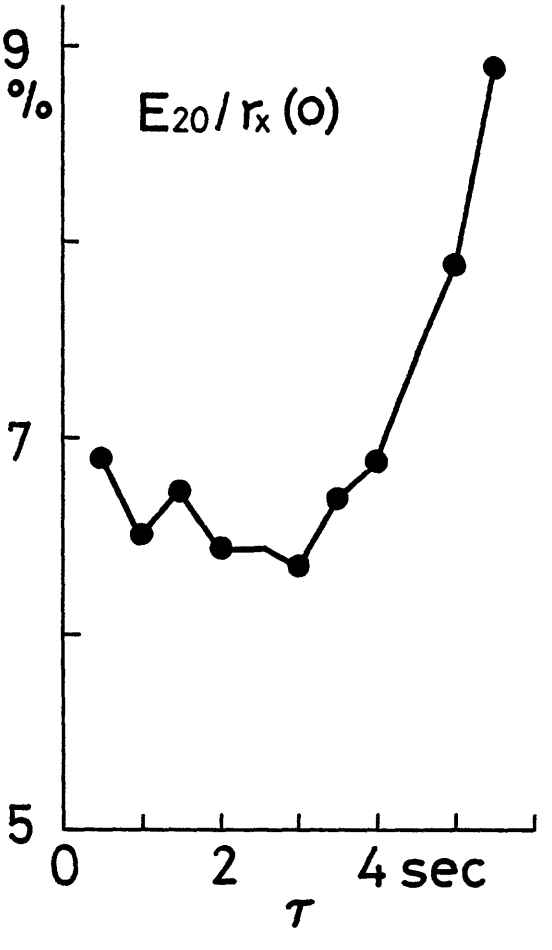

Figure 12

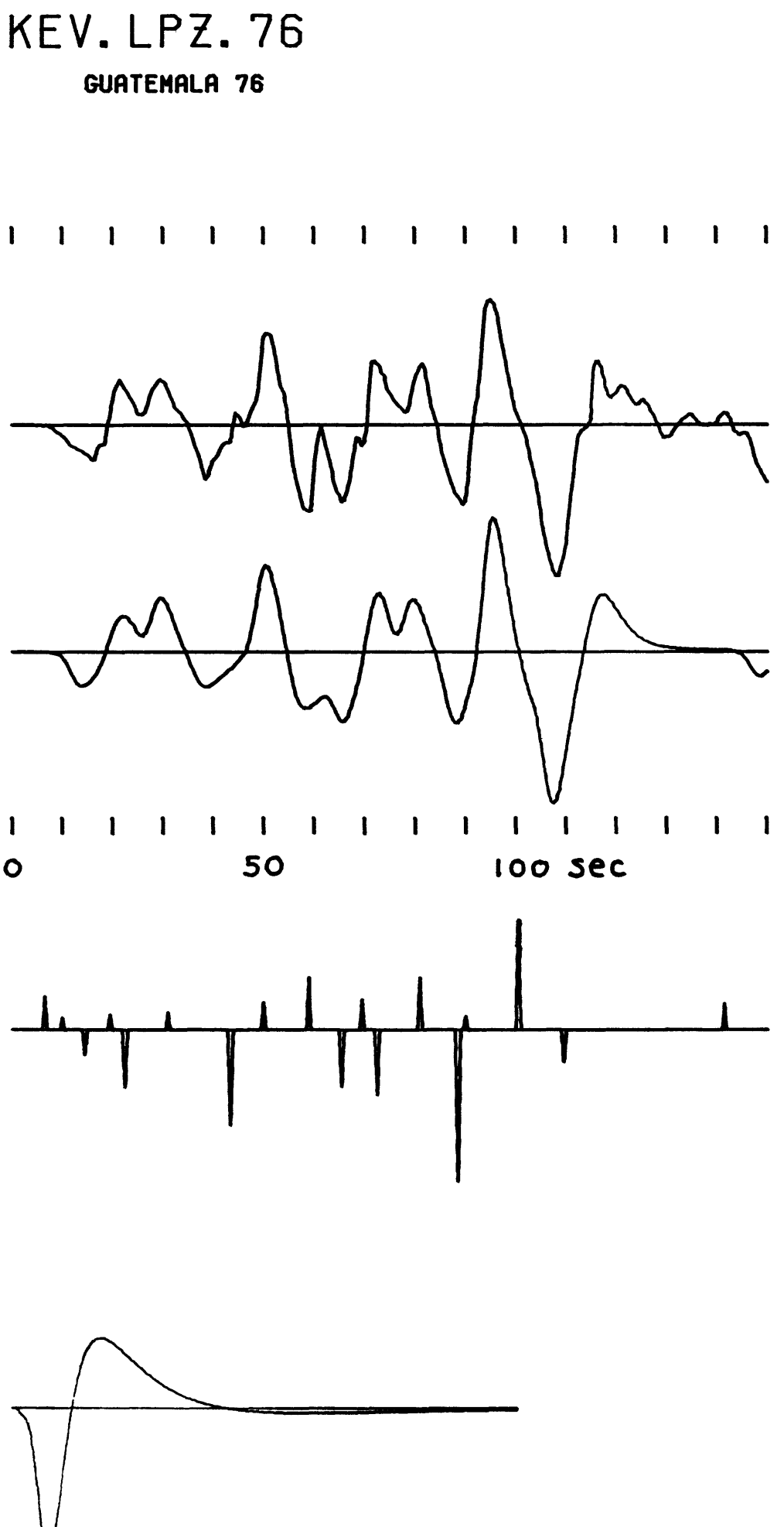

Figure 13a

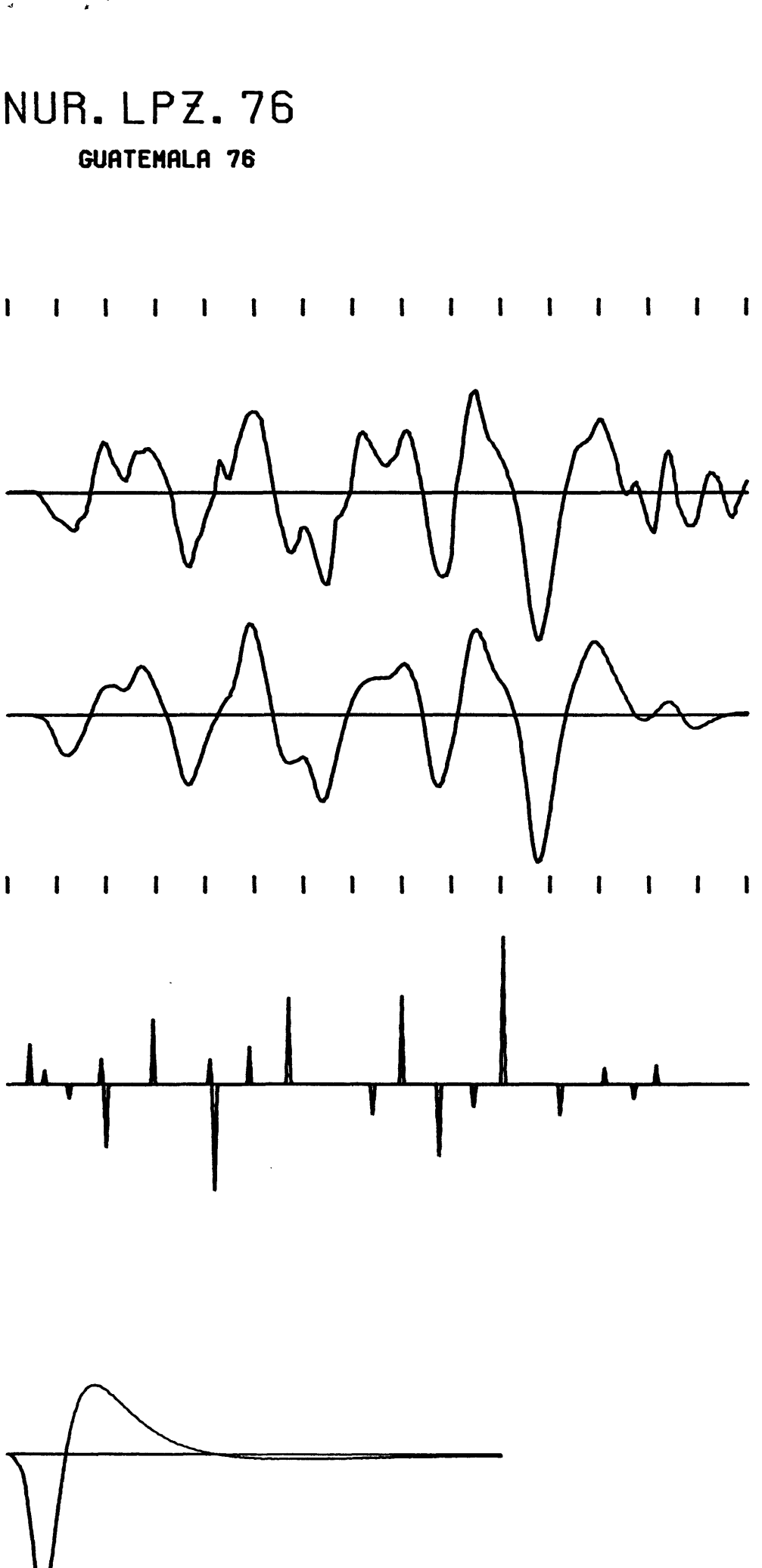

Figure 13b

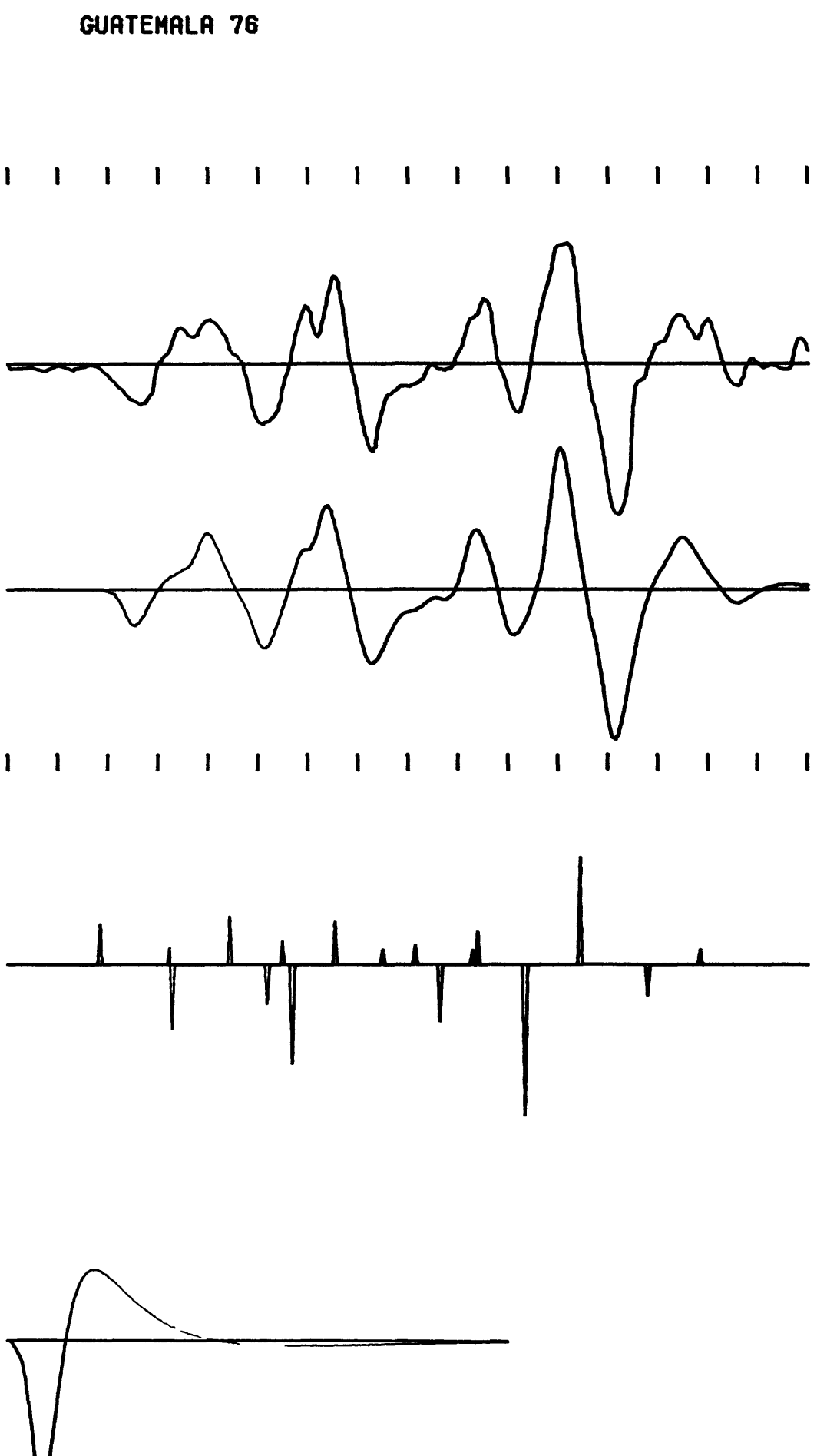

Figure 13c

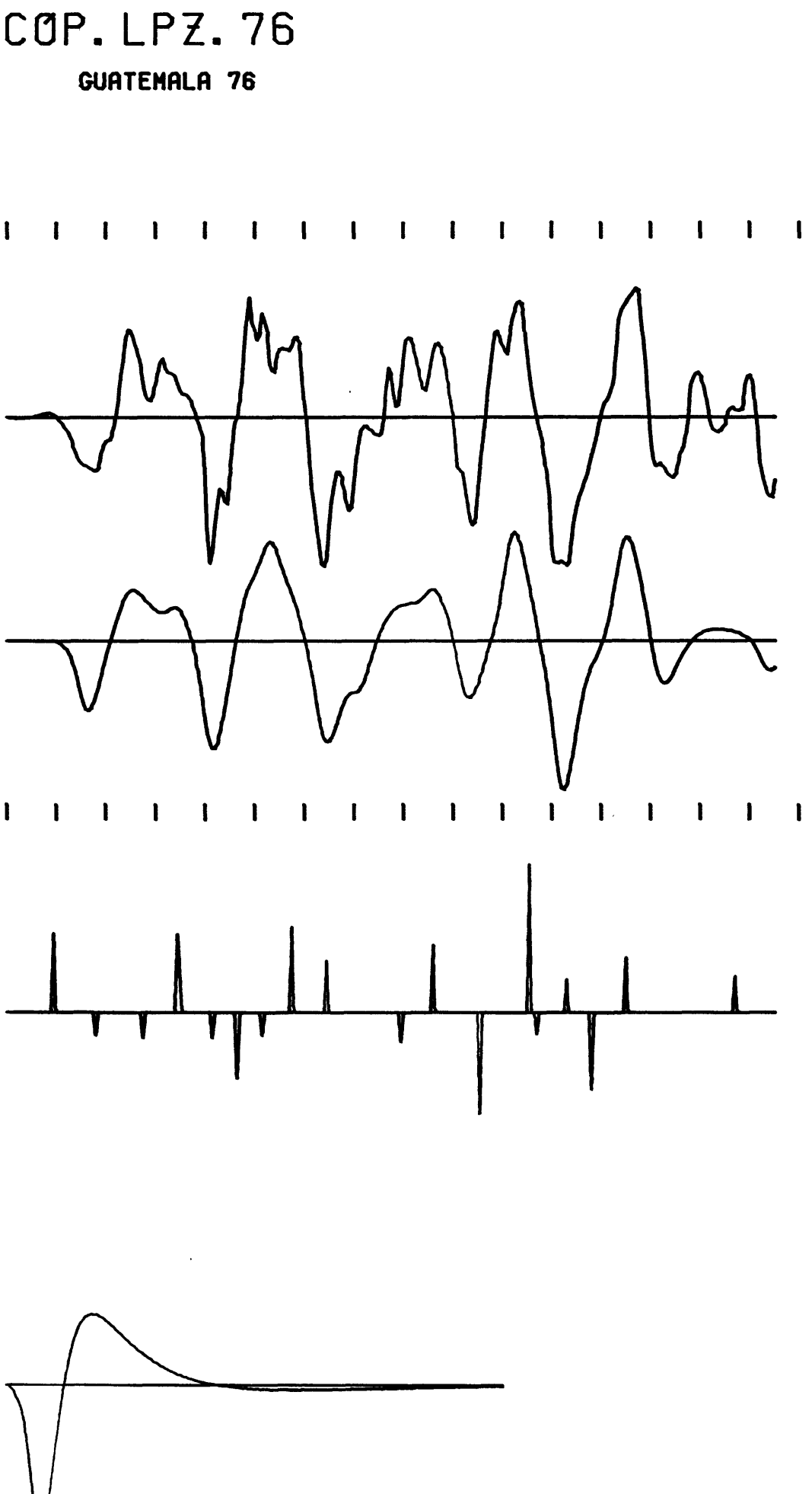

Figure 13d

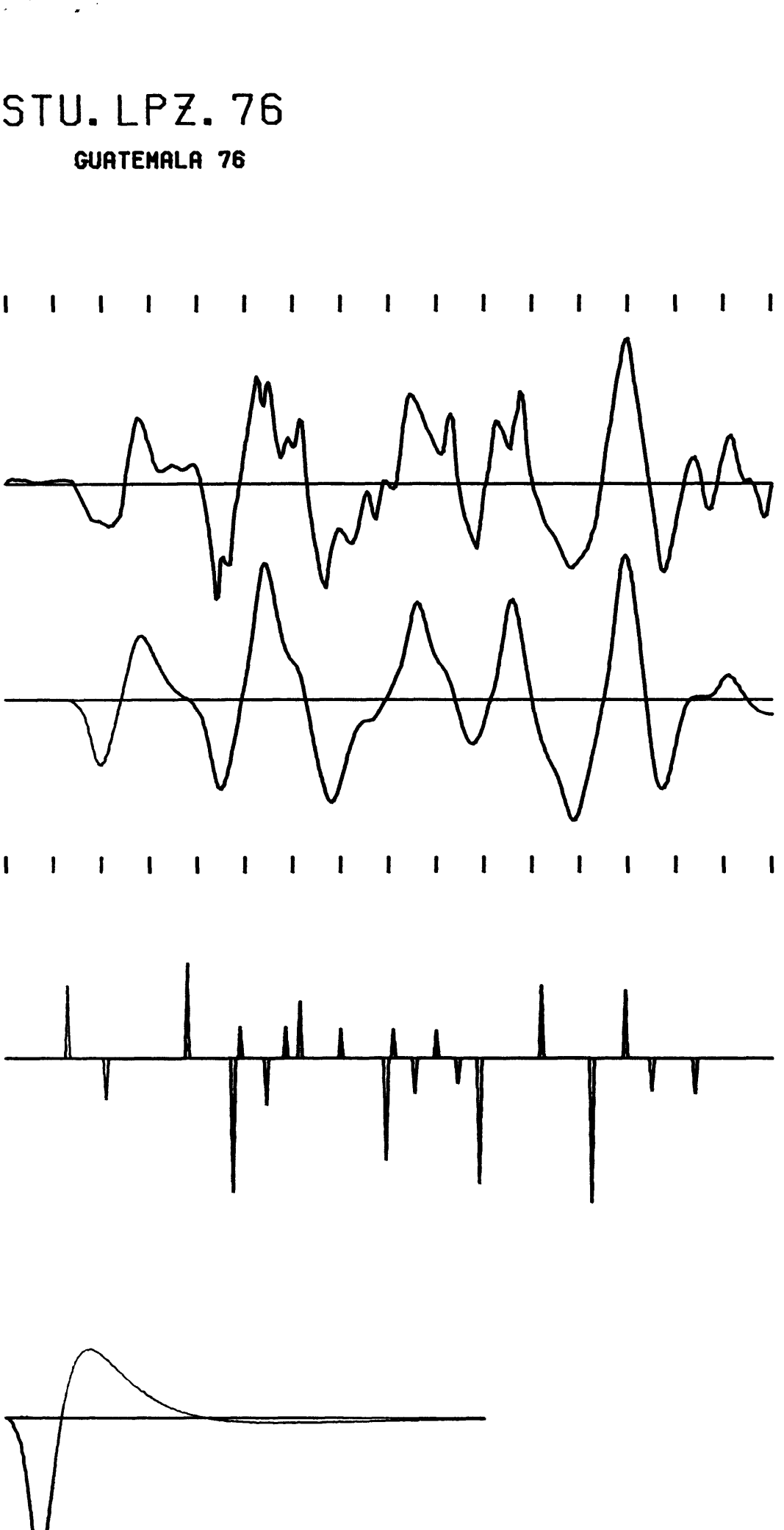

Figure 13e

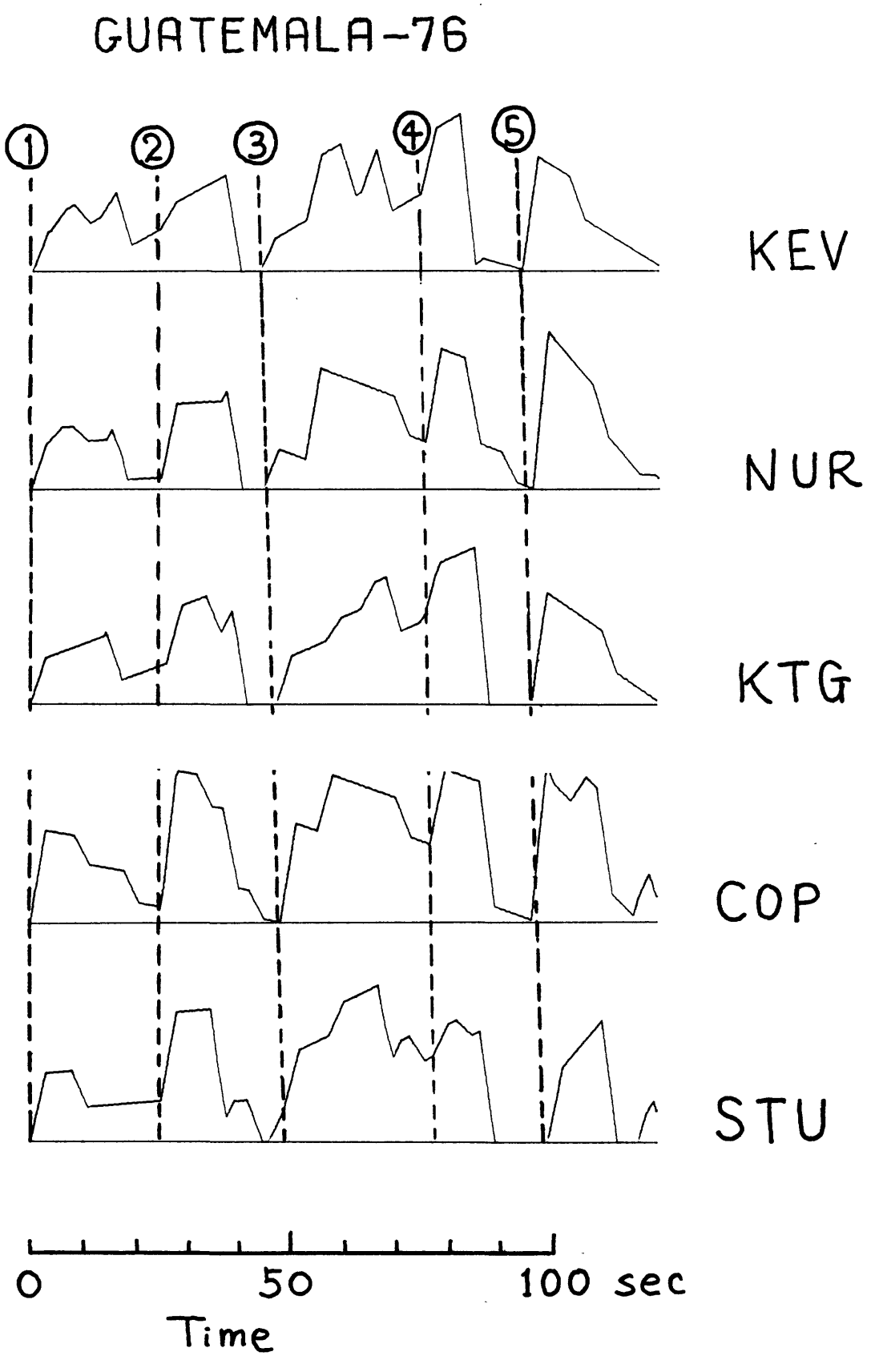

Figure 14

APPENDIX

VARIATION IN ASPERITY SIZE INFERRED FROM THE BODY WAVES OF GREAT EARTHQUAKES

Larry Ruff, (Seismological Laboratory 252-21, California Institute of Technology, Pasadena, CA 91125)
Hiroo Kanamori (same)

The regional variation in the behavior of seismic gaps and the seismic coupling of subduction zones can be interpreted as differences in the distribution of asperities on the fault plane. The rupture process of three of the largest earthquakes in this century (Kurile Is., M_W=8.5, 1963, Alaska, M_W=9.2, 1964, and Aleutian Is., M_W=8.7, 1965), is examined to investigate the nature of the asperity distribution. Since most of the direct P-waves from these events are off scale, the P-waves recorded in the core shadow zone are used, and are compared to the P-waves observed for a "typical magnitude 8" event (Niigata, M_W=7.6, 1964). The rupture process for the great earthquakes continues for many P-wave cycles and has a total duration $\geq$ 100 sec, while the Niigata earthquake consists of a single P-wave cycle. The characteristic period of the P-waves for the Alaskan earthquake is $\sim$ 60 sec, as opposed to $\leq$ 30 sec for the Niigata event, and the amplitude is an order of magnitude larger. The characteristic times for the Kurile Is. and Aleutian Is. events are intermediate. If the $\sim$60 sec characteristic time is interpreted as the breaking of individual asperities, then the characteristic asperity size scale is $\sim$200 km, larger than the characteristic length scale of the entire fault zone of the Niigata and other "magnitude 8" events. This indicates that the great earthquakes such as the Alaskan event are associated with a significantly larger asperity length scale.

1. Fall Meeting

2. 702934RUFF

3. Larry Ruff
   Seismo Lab
   Caltech 252-21
   Pasadena, CA 91125

4. S (Seismology)

5. none

6. O (Oral)

7. none

8. Bill to:
   Seismological Lab
   Caltech 252-21
   Pasadena, CA 91125

   P.O. 66-522478

   Student rate applicable

9. C